Annales Geophysicae (2002) 20: 1943–1958 © European Geosciences Union 2002

Annales Geophysicae

A statistical study of ion energization at 1700 km in the auroral region

M. Hamrin[1], **P. Norqvist**[1], **T. Hellström**[2], **M. André**[3], **and A. I. Eriksson**[3]

[1]Theoretical Physics, Umeå University, SE-901 87 Umeå, Sweden
[2]Department of Computing Science, Umeå University, SE-901 87 Umeå, Sweden
[3]Swedish Institute of Space Physics, Uppsala Division, Box 537, SE-751 21 Uppsala, Sweden

Received: 12 April 2002 – Accepted: 27 June 2002

Abstract. We present a comprehensive overview of several potentially relevant causes for the oxygen energization in the auroral region. Data from the Freja satellite near 1700 km altitude are used for an unconditional statistical investigation. The data are obtained in the Northern Hemisphere during 21 months in the declining phase of the solar cycle. The importance of various wave types for the ion energization is statistically studied. We also investigate the correlation of ion heating with precipitating protons, accelerated auroral electrons, suprathermal electron bursts, the electron density variations, K_p index and solar illumination of the nearest conjugate ionosphere. We find that sufficiently strong broadband ELF waves, electromagnetic ion cyclotron waves, and waves around the lower hybrid frequency are foremost associated with the ion heating. However, magnetosonic waves, with a sharp, lower frequency cutoff just below the proton gyrofrequency, are not found to contribute to the ion heating. In the absence of the first three wave emissions, transversely energized ions are rare. These wave types are approximately equally efficient in heating the ions, but we find that the main source for the heating is broadband ELF waves, since they are most common in the auroral region. We have also observed that the conditions for ion heating are more favourable for smaller ratios of the spectral densities S_E/S_B of the broadband ELF waves at the oxygen gyrofrequency.

Key words. Ionosphere (auroral ionosphere; wave propogation) Magnetospheric physics (electric fields)

1 Introduction

About 30 years ago it was discovered that the magnetospheric plasma includes a significant amount of plasma which has to be of ionospheric origin (Shelley et al., 1972). Since then, many spacecraft observations have confirmed that ionospheric ions, heated perpendicular to the divergent geomagnetic field through wave-particle interactions, can move adiabatically up the field lines and form so-called conics in the velocity distribution. Ions sufficiently energetic to escape the Earth's gravitational field flow out of the ionosphere and supply the upper magnetosphere with a considerable fraction of its plasma. The net oxygen loss from the ionosphere can be estimated to 10^{25} to 10^{26} ions/s, and there is a similar net loss of lighter H^+ ions from the ionosphere (Yau and André, 1997). However, a recent study has shown that the net O^+ loss can be considerably smaller due to a significant return flux of plasma from the magnetosphere to the ionosphere (Seki et al., 2001). The outflow of molecular ion species has been investigated by, for example, Lennartsson et al. (2000). The heated ions have a typical energy of a couple of eV to a few keV, and they have been observed at altitudes from a few hundred km by rockets (Whalen et al., 1978; Kintner et al., 1992) to a few Earth radii by satellites (Sharp et al., 1977; Lundin and Eliasson, 1991; André and Chang, 1993; Sauvaud et al., 2001).

Many different energizing mechanisms can be identified, some of which act at the same time in some regions, while others act separately. Investigating the wave-particle interactions responsible for the ion energization is important for understanding the ion outflow from the Earth's ionosphere, but also from the ionospheres of other planets. Transverse energization of ions can at least, in principle, be caused by the perpendicular component of waves in some frequency range, from much below the ion gyrofrequency (Hultqvist, 1996) to above the lower hybrid frequency (Chang and Coppi, 1981). It has also been suggested that ions could be heated directly by their nonadiabatic motion in electrostatic structures alone, without the need for time varying fields (Mishin and Banaszkiewicz, 1998).

At least at altitudes from 1000 km up to several 1000 km, a great deal of this energization is associated with broadband waves (sometimes called broadband extremely low-frequency waves (BB-ELF); Knudsen et al., 1998)). These waves are electric and magnetic field fluctuations observed in a broad frequency range of a few Hz to a few kHz in the spacecraft reference frame, and they are often found in the

Correspondence to: M. Hamrin (hamrin@space.umu.se)

auroral region. Perpendicular ion energization has often been observed in the presence of BB-ELF waves (Norqvist et al., 1996; André et al., 1998). Since these waves are usually present in a frequency range around the ion gyrofrequency, it is plausible that BB-ELF waves can heat ions. A simple model (Chang et al., 1986) shows that gyroresonant heating by left-hand polarized waves, with wave lengths much larger than the ion gyro radius and at frequencies near the ion gyrofrequency, can be an efficient energizing mechanism. Also, electromagnetic ion cyclotron (EMIC) waves have shown to be able to heat, for example, O^+ ions (Ashour-Abdalla et al., 1988). Waves (high above the ion gyrofrequency) around the lower hybrid frequency can also be efficient in energizing oxygen ions. However, for the waves to be in resonance with the gyrating ions, the ions must sometimes be pre-heated to some eV by, for example, BB-ELF waves (André et al., 1994). Moreover, magnetosonic waves with a sharp, lower frequency cut off just below the proton gyrofrequency (in the following denoted MSC waves; Hamrin et al., 2001) are proposed to be able to heat ions (Le Quéau et al., 1993; Rauch et al., 1993). However, these waves are often too weak to cause intense ion heating (André et al., 1998).

Overviews of observations of ion energization in the Earth's magnetosphere and of probable heating mechanisms can be found in André (1997), André and Yau (1997), Yau and André (1997), Chappell et al. (2000), Schunk (2000), and references therein. In the literature there is a long list of investigations of the wave-particle interactions causing the ion energization. However, many of these are mainly case studies focusing on the effect of a single wave type. Hence, there is a lack of comprehensive statistical studies, including several common waves types and properties of the plasma potentially relevant for the ion heating. Among the few statistical investigations correlating more than one wave type with ion energization events is the one by André et al. (1998) who used data from the Freja satellite to conduct a detailed statistical investigation of 20 O^+ ion heating events. BB-ELF waves were found to be the main causes for the most common type of the ion energization. Lund et al. (2000) used data from the FAST satellite to conclude that BB-ELF waves and EMIC waves are the main cause for the transverse energization at 2000 km altitude, while lower hybrid waves are much less important. Data from the Akebono satellite were employed by Kasahara et al. (2001) to investigate the occurrence of ELF/VLF waves and their correlation with transverse ion energization.

More than one wave type can energize the ions perpendicularly to the geomagnetic field. It is, therefore, important to investigate and compare the influences of the various waves on the ion heating in order to be able to elucidate the importance of the different energizing mechanisms. Conditions that are assumed to be directly responsible for the heating are in the following isolated from those that are seemingly influencing the ion energization, but which, in reality, are only indirect causes for the heating through the presence of the energizing waves.

In this article we conduct a statistical study to systematically and unconditionally investigate a set of different factors potentially influencing the ion energization. We present a comprehensive overview of ion energization in the presence of several wave types at frequencies relevant for ion energization. The wave types we focus on are BB-ELF waves, EMIC waves, MSC waves, and waves with frequencies around the lower hybrid frequency, all of which are often observed in the auroral region of the terrestrial magnetosphere. We also statistically investigate the importance of precipitating protons, accelerated auroral electrons, and suprathermal electron bursts for the ion energization. Moreover, we study the influence on the ion heating of the electron number density, the magnetic activity (K_p index), and the solar illumination on the nearest ionospheric foot-point of the flux tube crossed by Freja.

The instrumentation and our data are discussed in Sect. 2. Section 3 and 4 contain a brief description of the different wave types and particle distributions included in our study. The statistical analysis can be found in Sect. 5, and in Sect. 6 we briefly discuss and summarize our results.

2 Instrumentation and data

The joint Swedish and German satellite Freja (Lundin et al., 1994a,b) had a set of high resolution field and particle instruments and an auroral imager for studies of space plasma wave-particle interaction processes. We use data from the hot plasma instrument (F3H), the wave and plasma density instrument (F4), and the F7 electron spectrometer on Freja, to study various factors influencing the ion energization in the auroral region. Freja passed this region at an altitude of approximately 1700 km, and the orbit had an inclination of about 63°. In this study we use data only from the Northern Hemisphere. The low-inclination orbit makes data from the Freja satellite suitable for investigations of auroral phenomena, since the spacecraft, at times, moved along the auroral oval instead of across it. The satellite was Sun-pointing and spin stabilized with a spin period of 6 s.

2.1 Freja instrumentation

The Freja F3H hot plasma instrument included the Three-dimensional Ion Composition Spectrometer (TICS) (Eliasson et al., 1994b). TICS consisted of a spherical top-hat electrostatic analyzer with a 360° field of view, followed by a cylindrical magnet momentum analyzer with 32 angular sectors. TICS measured perpendicular to the satellite spin plane, giving three-dimensional distributions every 3 s. We focus mainly on the O^+ ions, but H^+ ion data are also included.

Waldemark and Norqvist (1995) have shown that a few percent of the ion data observed by Freja can be detected in the wrong ion mass channel. Inspecting our ion data in detail and studying a frequently occurring wave cut off in a two-ion plasma, we generally find that the plasma at Freja altitudes consists mainly of O^+ ions. For ion energies up to a few 100 eV (which are relevant for the O^+ energiza-

tion), the number of H^+ ions that is incorrectly detected in the O^+ mass channel is hence negligible compared to the total amount of detected O^+ ions. However, at these energies, the H^+ ion data are less accurate and are not used in this study. At higher energies (e.g. during precipitating proton events in the cusp/cleft region), the plasma is dominated by H^+ ions and, therefore, the error in the proton observations is negligible. In this investigation we use only proton data at energies higher than approximately 100 eV.

The wave and plasma density instrument F4 (Holback et al., 1994) used three pairs of electrostatic probes in the spin plane, with an antenna length of 21 m (two almost orthogonal pairs) and 11 m (one pair), to observe electric field fluctuations up to 13 kHz. Normally, the shorter boom pair was used for probe current measurements at a fixed bias voltage (Langmuir probe mode) for electron density estimation. In addition, a short (1.2 m) antenna was used for measurements up to 4 MHz. For observations of magnetic fields, F4 included three orthogonal search coil magnetometers on a 2-m stiff boom. The F4 telemetry was divided into different channels, where the sampling rate was 128 samples/s for the density channel (DC), 4 ksamples/s for the low-frequency (LF) electric and magnetic field channel, 32 ksamples/s for the medium-frequency (MF) channel, and 8 Msamples/s for the high-frequency (HF) channel. The wave forms were transmitted to ground after band-pass filtering and digital sampling. Due to limited telemetry rates, only the DC channel was continuously sampled. For the LF, MF, and HF channels, F4 transmitted brief snapshots of data with blank periods in between. Depending on the total telemetry rate, the duty cycle was 19–38% for the LF channel, typically with 750 ms or 1500 ms of data transmitted for each interval of 4 s. The corresponding duty cycles for the MF and HF channels were a few percent and a few hundredths of percent, respectively. Due to on-board filters, the LF electric and magnetic wave fields are damped below approximately 5 Hz and 30 Hz, respectively.

In this study we measure the component of the magnetic wave field that is along the spin axis, which is generally perpendicular to the background geomagnetic field. For the electric wave field we measure one component in the spin plane. Assuming that the spin axis and the true magnetic wave field are coplanar and both perpendicular to the geomagnetic field, the true magnetic wave field is, on the average, $\sqrt{2}$ times the measured component. Also, assuming the electric wave field to be perpendicular to the geomagnetic field, the true electric wave field is 2 times the measured component.

The F7 instrument included the Two-dimensional Electron SPectrometer (TESP) (20 eV to 25 keV) with a top-hat electrostatic analyzer, giving a 360° field of view (Boehm et al., 1994). However, in this study we use only data from the most field-aligned sectors.

2.2 Overview data sets

From the original time series of the F4 instrument, a reduced data set, consisting of the electron density and the electric and magnetic field power spectral densities, was created to provide an overview of the data at a reduced time resolution of a few fractions of a second. The electron density was estimated from the Langmuir probe current, calibrated (approximately accurate within a factor of two) by identification of the plasma resonance.

Similarly, another overview data set with a reduced time resolution was constructed. This reduced set contains the particle count rate versus electron energy (20 eV to 20 keV) from the sector of TESP covering the most field-aligned downward moving electrons, and the TICS count rates versus ion energy (1 eV to 4.2 keV) and pitch angle. Only data from the two neighbouring sectors pointing perpendicular to the spin axis are used. These overview data sets are available on disc and are thus convenient for statistical investigations. In this study, we use 21 months of such overview data from the Freja orbit 1152 to 9571 (from 1 January 1993 to 30 September 1994) in the declining phase of the solar cycle.

2.3 Wave and particle data

The electric wave field and electron density overview data from the F4 instrument were used in a preceding investigation and are discussed more thoroughly in Hamrin et al. (2001). The wave data were sorted into 13 approximately logarithmically spaced frequency bins for the LF (16 Hz – 1340 Hz) and MF (128 Hz – 10.7 kHz) channels, respectively. In addition to the data used in Hamrin et al. (2001), overview data of the magnetic wave field and the electrons, protons, and oxygen ions (from the F4, F3H, and F7 instruments) will be used in this study to investigate the important wave-particle interactions in the auroral region. Magnetic wave field data are sorted into the same frequency bins as the electric field data. The time resolution used for all of these data is 6 s, which is equal to the satellite spin period.

Compared to the original electron and ion overview data discussed in Sect. 2.2, the resolution has been reduced in this study. The TICS ion data have been sorted into four bins for each 6 s satellite spin, depending on pitch angle (α) and azimuthal angle (ϕ). However, the perpendicular distribution of ions energized below the satellite is generally folded into a conical shape, due to the magnetic mirror force in the divergent geomagnetic field. To include this effect, we use different sizes of the parallel and the anti-parallel bins. For the same reason we also choose not to center the perpendicular bins on $\alpha = 90°$. The four used bins are: one mainly field-aligned bin ($0 < \alpha < 60°$, $\forall\phi$), one mainly anti-parallel ($130° < \alpha < 180°$, $\forall\phi$), and two perpendicular bins ($60° < \alpha < 130°$) at azimuthal angles (ϕ) with 180° separation and ranging over approximately 30°. Ions rammed by the satellite motion can often be detected in one of the perpendicular bins when the satellite velocity is mainly perpendicular to the satellite spin axis and the geomagnetic

field (a commonly occurring situation for the Freja satellite). The ion (H^+ and O^+) data are sorted into 16 approximately logarithmically spaced energy levels between about 1 eV and 4 keV.

In the overview data base only data from the most field-aligned angular sector of TESP are used for the electrons. For each satellite spin in this study we average four 1.5-s-long energy spectra at 15 approximately logarithmically spaced energy levels between about 20 eV and 20 keV.

The wave and particle data are combined into a large data base by collecting the electric and magnetic field spectral densities, electron density, O^+, H^+, and electron energy spectra for each satellite spin of 6 s. Also, information about the K_p index, the universal time (UT), and the position of the satellite is included. Furthermore, from the satellite location and UT we determine whether the ionospheric foot-point in the Northern Hemisphere of the flux tube passed by Freja is sunlit or not. The K_p index can be used as an indication of the magnetic activity in the magnetosphere; it ranges between 0 and 9, and higher values of the index correspond to more intense disturbances.

The total number of satellite spins used in this investigation is more than 300 000. However, due to varying operating modes of the instruments, particle and wave data are not always available simultaneously. Therefore, data from some spins have been discarded in some parts of our study, while retained in others. Essentially, all the observations are obtained at altitudes between 1400 km and 1750 km, with the majority of the spins occurring around 1700 km. The corrected geomagnetic latitude (CGLAT) of the spins range from 40° to 75° (the lower limit is set by the coverage from the Esrange and Prince Albert ground stations and the upper limit is set by the 63° inclination of the orbit). At the altitudes and latitudes of our study, the difference between CGLAT and INV (the invariant latitude) is small. Hence, since INV is a more commonly used concept, we use this instead of CGLAT.

3 Wave classification

Whether the dispersion relations are known or not, we investigate the electric field power spectrum and associate the spectral features with various wave emissions. We will focus on the following four wave types: (1) BB-ELF waves, (2) EMIC waves, (3) MSC waves, and (4) waves with a spectral peak around the lower hybrid frequency. We use the electric field data from the LF channel to identify BB-ELF waves, EMIC waves, and MSC waves, and the electric field data from the MF channel to identify waves around the lower hybrid frequency of the F4 instrument (see Sect. 2). A more thorough discussion of the wave types and their classification can be found in Hamrin et al. (2001), where a larger number of wave types were studied and various parameters influencing the wave occurrence were investigated. In this article we use a subset of these wave data, focusing on waves at frequencies relevant to the ion energization.

We are working with overview data of the spectral density and do not access the original time series. In addition, we do not have any information on the $\boldsymbol{k}$ vectors. This choice constrains us to classify the various wave types only by looking for signatures in the power spectrum. Hence, it is difficult to identify a wave when strong emissions of other waves are present in the same frequency range. On the other hand, since there may be spectral features present at different frequencies in the power spectrum, more than one wave type can be classified for the same satellite spin.

Chang et al. (1988) and Retterer et al. (1989) found that waves with the same electric field spectral densities are approximately equally efficient in heating ions. Hence, unless otherwise stated, we focus on electric field spectral densities, S_E, at the relevant frequencies larger than 0.01 $(\mathrm{mV/m})^2/\mathrm{Hz}$ for the BB-ELF waves, the EMIC waves, and the waves around the lower hybrid frequency. However, since the MSC waves are usually much weaker than the other three wave types, we only require $S_E > 0.001$ $(\mathrm{mV/m})^2/\mathrm{Hz}$ for these waves.

3.1 BB-ELF waves

Broadband, extremely low-frequency (BB-ELF) waves have been investigated by, for example, Gurnett et al. (1984), who used data from the Dynamics Explorer 1 spacecraft and observed broadband, low-frequency electric and magnetic field fluctuations on essentially every low altitude pass over the auroral regions. Broadband ELF waves are often observed in regions with strong transverse ion energization, and they are found to be one of the most important sources of ion heating and ionospheric outflow, at least at altitudes of 1000 km to several 1000 km (André et al., 1998; Norqvist et al., 1998). As a measure of the strength of the BB-ELF waves, we will use in this article the electric field power spectral density at 28 Hz ($\approx f_{O^+}$, the oxygen gyrofrequency at the Freja altitudes). To include only waves that are sufficiently strong enough to cause significant ion heating, we focus on BB-ELF waves with a spectral density larger than 0.01 $(\mathrm{mV/m})^2/\mathrm{Hz}$. At these altitudes this spectral density corresponds to O^+ energies higher than a few eV (see Fig. 7 in André et al., 1998). Furthermore, in order to be classified as a BB-ELF wave, we also demand that the wave emissions in the range 48–412 Hz are strong enough. Hence, we require that the electric field spectral density does not fall off faster than $f^{-2.5}$. In our investigation we find nearly 17 000 spins where BB-ELF waves with $S_E > 0.01$ $(\mathrm{mV/m})^2/\mathrm{Hz}$ have been detected.

3.2 EMIC waves

Electromagnetic ion cyclotron (EMIC) waves have a clear peak in the power spectrum at frequencies below the proton gyrofrequency, and they are often generated by precipitating electrons (Temerin and Lysak, 1984; Gustafsson et al., 1990; Oscarsson et al., 1997). These waves are also believed to contribute to the ion energization (Vaivads et al., 1999). To identify EMIC waves from our wave data, we fo-

cus only on emissions with a single clear peak in the electric field spectral density in the range $0.1 f_{H^+} - 0.5 f_{H^+}$ (48–216 Hz), where f_{H^+} is the proton gyrofrequency (≈ 400 Hz at the Freja altitudes). Hence, we ignore the fact that EMIC waves can have several clear spectral peaks (Erlandson and Zanetti, 1998). Requiring that the spectral peaks must reach above 0.01 $(\mathrm{mV/m})^2/\mathrm{Hz}$ (wave emissions strong enough to be relevant for the ion energization), 115 spins have been classified as EMIC waves in our study.

3.3 MSC waves

Some ELF hiss spectra have a sharp lower cutoff at frequencies in the range 200 to 600 Hz (Gurnett and Burns, 1968). The observed cutoff is often just below the local proton gyrofrequency f_{H^+}, i.e. near 400 Hz at Freja altitudes, and is caused by the cutoff in the whistler mode dispersion relation in an oxygen dominated plasma containing both H^+ and O^+ (Rauch et al., 1993; Santolik and Parrot, 1999; Oscarsson et al., 2001). Such waves may be generated by anisotropic ion distributions at high altitudes in the equatorial region. As these waves propagate to lower altitudes, they may undergo resonant mode conversion, and the waves which have suitable polarization may be able to heat ionospheric ions (Johnson et al., 1989; Le Quéau et al., 1993, 1994). However, André et al. (1998) noted that these waves generally are too weak to cause intense ion heating. A sharp rise in the power spectral density just below f_{H^+} and a gradual decrease as a function of increasing frequency are identified as characteristic of a MSC wave in this study. In total, we have 7000 spins classified as MSC waves, where the maximum in the spectral density around f_{H^+} is larger than 0.001 $(\mathrm{mV/m})^2/\mathrm{Hz}$.

3.4 Waves around the lower hybrid frequency

Waves with spectral peaks in the lower hybrid frequency range are often observed in the terrestrial magnetosphere. According to their characteristics, these emissions are often classified as auroral hiss, saucers, chorus, and lower hybrid waves, all of which are often generated in the whistler mode (see André, 1997, and references therein). Auroral hiss can be generated by upward or downward moving electrons, and it can propagate both upwards and downwards from the region where it has been generated (Maggs, 1976; Sazhin et al., 1993). Saucers are often generated by upward moving field-aligned electrons in the return current region (Lönnqvist et al., 1993). Chorus seems to be generated by hot anisotropic electron distributions (Sazhin and Hayakawa, 1992). These waves all propagate on the whistler/lower-hybrid dispersion surface (André, 1985), on which we also find lower hybrid waves, though on this surface the latter waves should be confined to the lower hybrid plateau. To identify waves with a peak near the lower hybrid frequency, we focus only on single peaks occurring between $2 f_{H^+}$ and $26 f_{H^+}$ (896 and 10,720 Hz). Since the electron density is not extremely low, the lower hybrid frequency is rarely below $2 f_{H^+}$ in our study. Furthermore, since the plasma generally is not proton dominated (where the lower hybrid frequency theoretically can be up to $43 f_{H^+}$), we expect to find most of the waves within our frequency interval. In our study, 7400 spins have a peak higher than 0.01 $(\mathrm{mV/m})^2/\mathrm{Hz}$ near the lower hybrid frequency.

4 Particle classification

4.1 Energized ions

From our database of measurements of more than 300 000 spins, we have identified the spins characterized by ion energization perpendicular to the geomagnetic field. For this purpose we have used the method of k-Nearest Neighbours (kNN), which is suitable for automatic pattern classification from a large data set (see Desarathy, 1991, for a survey of the literature on this subject). This method is often known to be superior to other more sophisticated classification techniques. The major drawback with kNN is often an excessive use of computer power.

For each 6-s satellite spin, the available data for the oxygen ions are the count rates versus ion energy and pitch angle in 16×4 bins from the TICS instrument (see Sect. 2). These 64 values are used as coordinates in a 64-dimensional representational space to portray each spin. When the total count rate in all 64 bins is sufficiently low, we directly classify that spin as not associated with any ion energization. To eliminate the effects of the ion density shifting much between different spins, the sum of the count rates in the 64 bins is hereafter normalized to unity. The kNN method is then used for identifying those spins which are characterized by transverse ion heating.

To apply the method, the position of each unclassified spin in this normalized 64-dimensional space is compared to the positions of the spins comprising a larger known training data set. The training set is classified by hand and it consists of 120 examples of spins with perpendicular ion heating and 350 examples of spins with no ion heating (but with relatively high count rates at larger energies), respectively. The latter part corresponds, for instance, to events when precipitating ions are measured in the absence of perpendicularly heated ions, or when the spacecraft accidentally is charged to a few volts due to certain conditions in the space environment and hence, low energy ions are incorrectly observed at higher energies. If the unclassified spin is closest to one of the 120 examples of energized ions, we classify that spin as ion heating, while if it is closer to one of the other 350 examples, it is assumed not to be associated with ion heating. To measure the distances in this space, we use the so-called l_1-norm. Hence, the distance between two points in the 64-dimensional representational space is given by the sum of the absolute values of the coordinate distances.

O^+ ions at rest in the plasma frame will be observed in the satellite frame at an average energy determined by the satellite velocity. Freja moves approximately at 7 km/s, and this velocity corresponds to an O^+ energy of about 4 eV.

For the classification of the spins, we define ion heating as O^+ ions energized perpendicular to the geomagnetic field to more than 1–2 eV in the plasma frame (a numerical simulation of how different ion energies are observed in the Freja satellite frame can be found in Norqvist, 1995). Our method allows us to distinguish between energization in the plasma frame and energization in the spacecraft frame caused by the satellite velocity.

A detailed visual inspection of a few hundred spins randomly chosen out of our database shows that our algorithm missed less than 5% of the spins which were associated with true ion heating. The spins missed generally have energies just above the 1–2 eV limit. Out of the spins that our algorithm has classified as ion heating, more that 95% are indeed ion heating according to the visual classification. Thus, the total number of correctly classified ion energization spins agrees well with the detailed inspection, and more than 90% of the spins are classified identically by visual classification and by the kNN method.

4.2 Precipitating protons

Magnetosheath plasma (precipitating ions and electrons) are often observed at Freja altitudes, for example, in the cusp/cleft region, together with energized ions. However, precipitating protons with less energy flux can also be found on the nightside, sometimes coexistent with ion heating (Eliasson et al., 1994a). One explanation for the existence of ion heating in these regions is that precipitating protons can generate waves with frequencies around the lower hybrid frequency (Roth and Hudson, 1985).

For the identification of precipitating protons in our study, we do not need to use the KNN method, since the features we look for in our proton data are relatively easy to find. Therefore, a simpler algorithm than the KNN method is sufficient for localizing those spins which are associated with precipitating protons. For this purpose we require an increased count rate in the TICS proton channel (see Sect. 2) as a function of increasing energies above a few hundred eV. Furthermore, to distinguish this feature from intense perpendicular ion heating, the pitch angle distribution should not be that of an ion conic, and the O^+ data should not show signs of intense ion heating at the same energies. To eliminate the weakest events, we only classify events with an energy flux above approximately 10 μW/m^2. However, due to our low resolution in pitch angle, this value is just a coarse estimate.

A visual inspection of a few hundred randomly chosen spins shows an almost total agreement between the result from the above algorithm and that from the visual classification.

4.3 Auroral electrons

Downward moving auroral electrons accelerated by a field-aligned electric field to energies around or above one keV are sometimes observed simultaneously with energized ions. Wave emissions in frequency ranges relevant for the ion heating are also often measured at the same time. To identify which of the spins in our database are associated with inverted-V electrons, we use the kNN method once again. The reason for not employing a method similar to the one used to detect precipitating protons is that it is difficult to construct a simple algorithm that distinguishes these electrons from the electron population causing diffuse auroras.

For each 6-s spin, the count rate in four energy spectra at 15 different energy levels (see Sect. 2) represents the available data. This gives us a 60-dimensional representation space used when applying the kNN method on the electron data. For the classification we compare the unknown spins with a set of 77 examples of spins with auroral electrons and a set of 191 examples of spins without accelerated auroral electrons. To eliminate the weakest events, we require an energy flux of about 100 μW/m^2 or more.

4.4 Suprathermal electron bursts

Another electron distribution often correlated with ion energization is broadband in energy from tens to hundreds of eV (Knudsen et al., 1998). These electrons are often field aligned and usually occur on smaller spatial scales than the accelerated auroral electrons. These electrons were termed suprathermal electron burst (STEB) by Johnstone and Winningham (1982). STEB comprise a relatively broad class of electron precipitation, and similar to Knudsen et al. (1998), we do not focus on the details of the generation mechanisms and the velocity distributions. A suprathermal electron burst often coexists with precipitating protons in the cusp/cleft region but, also with energized ions on the nightside (see, e.g. Fig. 1 in André et al., 1998).

To classify a spin as characterized by a suprathermal electron burst, we require that the total count rate of the downward moving electrons measured by TESP (see Sect. 2) at energies below a few hundred eV is sufficiently high. The minimum count rate chosen for this study corresponds to a downward energy flux of about 1000 μW/m^2. Since we work with measurements of downward moving electrons, we do not consider contributions from the electron flux in the other direction.

5 Result and discussion

In this section we will investigate some wave-particle interactions potentially responsible for the oxygen ion energization at Freja altitudes in the auroral magnetosphere. We will study unconditionally the correlations between various potentially relevant factors for the ion energization. In particular, we will focus on the importance of the wave types on the ion heating, as discussed in the previous section (BB-ELF waves, EMIC waves, MSC waves, and waves around the lower hybrid frequency). Moreover, we will correlate the occurrence of energized ions with the presence of precipitating protons, accelerated auroral electrons and suprathermal electron bursts (see Sects. 3 and 4). Also, the effect of other

factors, such as the magnetic activity (the K_p index), the solar illumination of the ionosphere and the electron density, will be included in the study.

5.1 Statistical correlations of waves and particles

Table 1 shows the probability (in %) of observing the quantities listed in columns 1–10 in the presence of the particle distributions, wave types, and other characteristics indicated in rows 1–16.

Listed in the ten columns of Table 1 are the conditional probabilities of observing: (1) energized ions (denoted as "Heated O^+"), (2) precipitating protons with keV energies (denoted as "Prec. H^+"), (3) suprathermal electron bursts ("STEB"), (4) downward moving electrons with energies around or above 1 keV ("keV e^-"), (5) strong BB-ELF waves with an electric field power spectral density, S_E, larger than 0.01 $(\mathrm{mV/m})^2/\mathrm{Hz}$ at the O^+ gyrofrequency ("BB-ELF"), (6) EMIC waves with $S_E > 0.01$ $(\mathrm{mV/m})^2/\mathrm{Hz}$ ("EMIC"), (7) MSC waves with $S_E > 0.001$ $(\mathrm{mV/m})^2/\mathrm{Hz}$ at frequencies just below the proton gyrofrequency ("MSC"), (8) waves at frequencies around the lower hybrid frequency with $S_E > 0.01$ $(\mathrm{mV/m})^2/\mathrm{Hz}$ ("LH"), (9) a decreased electron density ($n/n_0 < 0.25$), and (10) an increased electron density ($n/n_0 > 4.0$).

The first row (denoted "All spins") shows the probability of observing the different particle distributions, wave types, or specific density conditions, given that the relevant instruments on board the satellite have measured the necessary quantities. These probabilities will be used mainly as reference when comparing with the other values in Table 1.

Column 1 on rows 2–9 contains the conditional probability of detecting energized ions coexistent with the particle distributions or wave types listed to the left. Similarly, the probability of observing ion energization during low or high magnetic activity ("$K_p < 3-$"and "$K_p > 4+$", respectively) or when the nearest ionospheric foot-point of the flux tube crossed by Freja is in sunlight ("Sun") or in shadow ("Shadow") can be found in rows 10–13. The following two rows contain information on the probability of detecting heated ions during conditions of electron density enhancements ("$n/n_0 > 4.0$") or electron density reductions ("$n/n_0 < 0.25$"). The density is considered increased (decreased) whenever the electron density normalized to the average density n_0 in the same MLT-INV-bin is found to be larger (smaller) than 4.0 (0.25). In the normalization of the densities, we have taken into account for each individual spin whether the ionosphere below Freja is sunlit or not. The bottom row includes only measurements above 65° INV ("INV $> 65°$"). Analogous to column 1, columns 2–10 contain similar conditional probabilities corresponding to various combinations of particle distributions, wave types, and other relevant plasma properties.

5.2 Ion energization and waves

Analyzing the first column of Table 1, we immediately observe that some of the most important factors influencing the ion energization include the presence of BB-ELF waves, EMIC waves, and waves at frequencies around the lower hybrid frequency. The probabilities of observing energized ions coexistent with theses waves are 13%, 20%, and 7.6%, which should be compared to the 1.3% probability of detecting ion heating among all spins included in the full database (row 1). Hence, for the same threshold value of the electric field spectral densities ($S_E > 0.01$ $(\mathrm{mV/m})^2$) we note that these three wave types are approximately equally efficient in heating ions. However, our result should not be interpreted to mean that all three wave types are equally important for the ion heating at the Freja altitudes, since BB-ELF waves are clearly occurring more frequently in our data than the EMIC waves and the waves around the lower hybrid frequency. This can be seen in columns 5, 6, and 8 of row 1 in Table 1. Moreover, from the same columns, but instead row 2, it is clear that BB-ELF waves are more common during ion energization than the other two wave types. Hence, we conclude that BB-ELF waves are the main source for the ion energization at Freja altitudes in the auroral region.

The MSC waves are also in the frequency range potentially relevant for the transformation of energy from the waves to the ions, but from Table 1 we see that the conditional probability of detecting energized ions is much smaller in the presence of MSC waves than in the presence of the other three wave types discussed above. In our entire database, we only find data from two spins where ion heating and MSC waves coexist. Moreover, in both of these cases, we also observe BB-ELF waves with larger electric field spectral densities than the MSC waves. MSC waves could, however, in principle, appear more often in the auroral region, but these emissions are impossible to detect in our data, since there usually are stronger and more energetic wave emissions present at the same time. Hence, we cannot find a single spin in our complete database where the MSC waves seem to be the main source of energy for the oxygen ion heating. André et al. (1998) suggested that MSC waves are generally too weak to cause substantial oxygen ion energization. Hence, this is in total agreement with our result stated in Table 1.

The presence of relatively strong waves that can be in resonance with the ions is the most likely direct cause for the ion energization detected by the Freja satellite. BB-ELF waves, EMIC waves, and waves around the lower hybrid frequency in Table 1 all seem to fulfill these requirements, while MSC waves are obviously insufficient for the heating. This agrees with previous results from, for example, Norqvist et al. (1998) and Lund et al. (2000).

5.3 Ion energization and electron density

Inspecting columns 1, 5, 6, and 8 and comparing with row 1, we see that the probabilities of observing heated ions, BB-ELF waves, EMIC waves, and waves around the lower hy-

Table 1. Conditional probability (in %) of observing various particle distributions, waves types, and electron density enhancements or reductions (listed in the title row) in the presence of the particle distributions, waves types, and other characteristics in the leftmost column (see the text for more details). Row 1 indicates the probabilities of detecting the wave and particle properties in the entire database of all satellite spins included in our study, given that the relevant instruments on board the satellite have measured the necessary quantities

Conditions	Particle distributions				Wave types				Density incr./decr.	
	1. Heated O^+	2. Prec. H^+	3. STEB	4. keV e^-	5. BB-ELF	6. EMIC	7. MSC	8. LH	9. $\frac{n}{n_0} > 4.0$	10. $\frac{n}{n_0} < 0.25$
1. All Spins	1.3	3.5	5.5	3.1	4.9	0.042	1.4	1.6	1.1	9.6
2. Heated O^+	—	21	50	12	51	0.65	0.065	9.4	1.5	21
3. Prec. H^+	7.6	—	34	0.96	15	0.048	1.1	9.3	5.7	4.1
4. STEB	11.8	22	—	9.2	21	0.10	0.51	3.2	3.6	4.1
5. keV e^-	5.0	1.1	16	—	7.3	0.63	0.11	3.2	1.7	7.9
6. BB-ELF	13	11	24	4.7	—	0.24	0.55	4.0	1.0	34
7. EMIC	20	4.0	13	48	28	—	0	36	0	42
8. MSC	0.060	2.8	2.0	0.24	2.0	0	—	1.9	0.38	2.2
9. LH	7.6	6.3	11	18	12	0.76	1.5	—	0.03	23
10. $K_p < 3-$	0.56	2.2	2.7	1.8	4.3	0.041	0.98	0.60	0.22	12
11. $K_p > 4+$	4.6	6.3	14	5.4	6.9	0.033	1.7	3.3	3.4	5.1
12. Sun	0.83	3.7	5.5	2.1	2.9	0.002	2.1	1.2	0.19	6.1
13. Shadow	2.2	3.0	5.5	5.1	8.7	0.12	0.080	2.2	2.7	16
14. $n/n_0 > 4.0$	1.7	19	19	5.0	3.8	0.0	0.46	0.04	—	—
15. $n/n_0 < 0.25$	2.8	1.6	3.6	2.7	18	0.19	0.3	3.5	—	—
16. INV $> 65°$	1.8	5.0	4.7	7.9	6.9	0.061	1.8	1.6	1.2	12

brid frequency are higher when the ionosphere below Freja is in the shadow (row 13) rather than in the sunlight (row 12). The probabilities are increased even further in the presence of electron density reductions of more than a factor of four ($n/n_0 < 0.25$ in row 15). The obvious explanation is that a reduced electron density is favourable to wave growth, and in the absence of ionizing solar illumination, the electron density is generally sufficiently low. Moreover, if the ionospheric foot-point of the flux tube crossed by Freja is sunlit, the electron density is higher and the conditions for wave growth are worse.

Hamrin et al. (2000) have shown that ion heating is stronger and more common in a low density plasma, for example, in the absence of solar illumination. As suggested by Rönnmark (1999), a low electron density forces the electrons to be accelerated to energies of several keV, in order to be able to carry an imposed field-aligned current between the ionosphere and the magnetosphere (note that this reasoning applies both to the upward and downward current regions), thereby making the conditions favourable for wave growth. Moreover, due to their increased magnetic moment, the ions heated by the waves can escape towards higher altitudes in the divergent geomagnetic field, hence, reducing the density further and improving the conditions for wave generation in a feedback loop (Hamrin et al., 2000). Also, since we denote by ion heating an average energy per particle larger than a few eV (see Sect. 4), it is obvious that the ion energy density must be higher for a dense plasma than for a tenuous plasma, to correspond to the same ion energy. Therefore, it is reasonable to assume that the energy in the waves available for the energization must be higher if the plasma is dense.

From the discussion in the previous section we do not expect MSC waves to contribute to the ion heating. This is consistent with Table 1, since MSC waves are clearly less common in the absence of solar illumination (row 12) and in a plasma of decreased electron density (row 15) than in the full database (row 1).

From row 14 in Table 1 we can also conclude that the probability for ion energization is increased in regions of enhanced electron density ($n/n_0 > 4.0$). However, from columns 9 and 10 of row 2 we clearly see that density depletions are much more common than density enhancements when we are observing ion energization. We do not believe that the high probability of ion heating in a plasma of $n/n_0 > 4.0$ indicates that an enhanced electron density is favourable for the ion energization. The increased probability is most likely caused by the ion heating in the cusp/cleft region, on field lines, where solar wind plasma has access to low altitudes, which increases the density. This has been confirmed by examining in detail some of the ion heating events included in our study. By inspecting columns 2 and 3, we also see that both precipitating H^+ and suprathermal electron bursts (STEB), which are typical for the cusp/cleft region, are more common in regions of density enhancements (row 14). From columns 5–8 we, moreover, note that none of the waves at frequencies relevant for energizing the oxygen ions seem to become more frequent when $n/n_0 > 4.0$. However, when only focusing on strong waves (not shown in Table 1) with electric field power spectral densities larger than 0.1 $(\mathrm{mV/m})^2/\mathrm{Hz}$ (instead of 0.01 $(\mathrm{mV/m})^2/\mathrm{Hz}$ as was used in

preparing Table 1), we observe BB-ELF waves in 0.81% of the spins of the entire database and in 0.89% during density enhancements (3.2% at density reductions). Hence, we see a slightly increased probability of observing strong waves in the presence of density enhancements. Moreover, if we, in addition, focus on the magnetic field spectral density component of the BB-ELF waves, we find that the probability of detecting strong wave emissions (magnetic field spectral densities at the O^+ gyrofrequency larger than 10^{-3} $(nT)^2/Hz$) in regions of increased electron density is 1.5%, while it is 0.055% in regions of density reductions. This should be compared with the probability of 0.55% of finding these emissions in the entire database. Note that these data are not shown in Table 1. André et al. (1998) used Freja data to show that the ratio between the electric and the magnetic fields at the oxygen gyro frequency is smaller in the cusp/cleft region than in other regions of strong BB-ELF wave emissions. They also concluded that these waves can often be regarded as electromagnetic in this region. The importance of the magnetic wave field will be investigated further in Sect. 5.8.

5.4 Auroral electrons

From Table 1 we also observe that accelerated auroral electrons and ion heating are relatively strongly correlated. Moreover, auroral electrons are more common above an ionosphere in the shadow than one in the sunlight, which is consistent with Newell et al. (1998) and Hamrin et al. (2000). From columns 9 and 10 (row 1) in Table 1 we note that strong electron density depletions of a factor of four are common in our data.

When Freja passed field lines with downward accelerated auroral electrons, one may expect that the electron density should be reduced (McFadden et al., 1999). However, from Table 1 (row 5 and column 9), we see that density enhancements are common when auroral electrons are observed. This can be explained by the fact that Freja often passes well below the acceleration region at lower altitudes where the electron density can be enhanced by backscattered and secondary electrons (Evans, 1974). Furthermore, at Freja altitudes, the most intense ion heating, and, therefore, the corresponding density reductions, are often observed just outside the region of auroral electrons (André et al., 1998).

5.5 Ion energization versus MLT and INV

From the last row of Table 1 it can be seen that ion heating and the related processes are more frequent at high invariant latitudes (INV $> 65°$). However, to obtain a more complete understanding of where the ion heating and the processes (directly and indirectly) responsible for the energization are active, we need to investigate the occurrence frequency (under the relevant conditions) plotted versus MLT and INV.

In Fig. 1 the occurrence of ion energization versus MLT and INV is presented. Since no single spin with ion heating was detected below 50° INV in the entire database, we only focus on $50° \leq \text{INV} \leq 75°$. The logarithmic colour scale

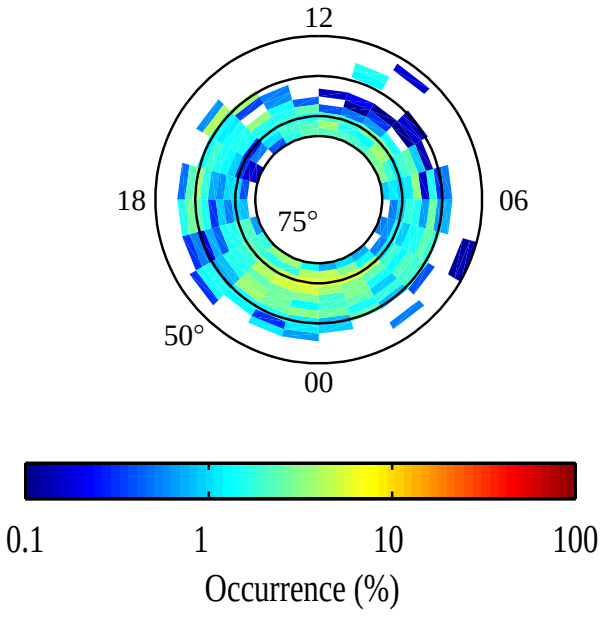

Fig. 1. Occurrence of ion energization versus MLT and INV. The locations of 50°, 60°, 70°, and 75° INV are indicated with solid lines.

ranges from 0.1% (blue) to 100% (red). The data are sorted into bins of size 0.5 h and 2° INV. We see that ion heating is most common on the nightside around 70° INV. We also note that ion energization is relatively frequent at high latitudes in the pre-noon sector, for example, the cusp/cleft region. This result is consistent with Fig. 4 in Hamrin et al. (2001) (first published in Norqvist, 1998). The ion data from Norqvist (1998) were also used by Norqvist et al. (1998), where it was shown that the outflow of oxygen ions, on the other hand, is the largest between 9:00–12:00 MLT (the cusp/cleft region) on the dayside. The ion outflow can be higher on the dayside simply because the plasma density is higher in this region.

5.6 Ion Energization and waves versus MLT and INV

In Figs. 2a and b, we present the probability of detecting ion heating in the presence of BB-ELF waves (with $S_E > 0.01$ $(mV/m)^2/Hz$ at the oxygen gyrofrequency) and waves around the lower hybrid frequency ($S_E > 0.01$ $(mV/m)^2/Hz$), respectively. The MLT-INV bins and the colour scale are the same as for Fig. 1. When comparing with Fig. 1, we note that BB-ELF waves increase the probability of observing energized ions at all MLT and INV. As discussed in Hamrin et al. (2001) the waves around the lower hybrid frequency appear in two distinct regions: one high-latitude band (about 70° INV) in the evening and night sector, and one morning and dayside band at lower latitudes (about 60° INV). From Fig. 2b we note that the oxygen ion energization correlates with the high-latitude band.

Since EMIC waves are quite rare in our study (EMIC waves are only detected in 115 spins), we do not have enough

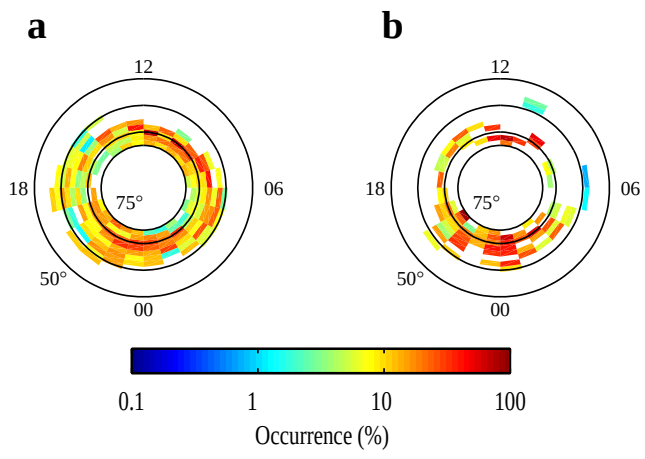

Fig. 2. Probabilities of detecting energized ions versus MLT and INV in the presence of (**a**) BB-ELF waves and (**b**) waves with frequencies around the lower hybrid frequency (see Sect. 3 for an exact definition of the waves). The locations of 50°, 60°, 70°, and 75° INV are indicated with solid lines. The colour scale is the same as in Fig. 1.

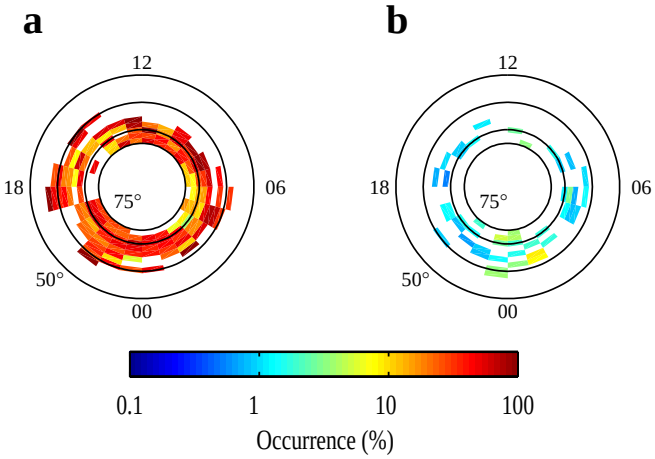

Fig. 3. Probabilities of detecting energized ions versus MLT and INV in the presence of (**a**) strong BB-ELF waves, strong EMIC waves, or strong waves around the lower hybrid frequency, and (**b**) no BB-ELF waves, no EMIC waves, and no waves around the lower hybrid frequency. The colour scale is the same as in Figs. 1 and 2.

statistics to analyze the EMIC data as a function of MLT and INV. However, we note that 20 of the 115 EMIC spins (for 100 EMIC spins there existed simultaneous ion measurements) coexist with ion heating.

To further investigate the importance of the three energizing wave types, in Fig. 3a we plot the occurrence of ion heating in the presence of strong emissions of BB-ELF waves, EMIC waves, or waves around the lower hybrid frequency (all with $S_E > 0.1$ (mV/m)^2/Hz at the relevant frequencies instead of 0.01 (mV/m)^2/Hz as was used in preparing Figs 2a and b). Note that the same scales are used in this figure as in Figs. 1 and 2. When comparing Figs. 1 and 3a we see that the presence of these wave types substantially increases the probability of observing heated ions. On the contrary, in requiring that none of these three wave types be stronger than $S_E > 10^{-3}$ (mV/m)^2/Hz (at the relevant frequencies), ion heating is very seldom detected. This can be seen from Fig. 3b. Hence, we conclude that the presence of BB-ELF waves, EMIC waves, or waves around the lower hybrid frequency represent the main causes for the oxygen ion energization at the Freja altitudes in the auroral region.

However, the few cases when strong enough energizing waves are not observed in the absolute vicinity of the heated ions, do not necessarily indicate that the waves are not the main cause for the heating. Instead, it is possible that the wave emissions have turned off, leaving the heated ions behind in the absence of any energizing waves. Another possibility is that the regions where the waves energize the ions move relative to the ions, or that the heated ions drift away from the regions of strong wave emissions (André et al., 1990; Knudsen et al., 1994; Norqvist et al., 1998).

5.7 Other particle distributions and characteristics versus MLT and INV

Inspecting column 1 of Table 1, apart from the energizing waves, there are also a number of other factors which appear to influence the conditions for the ion heating. These are the particle distributions and the other properties listed in rows 3–5, and 10–16 of column 1. However, this should not be interpreted as if these plasma characteristics are the direct cause for the ion energization. Instead, most of these can be considered as indirect consequences of, or indirectly related to, the presence of BB-ELF waves, EMIC waves, or waves around the lower hybrid frequency, which are primarily responsible for the ion heating.

In Fig. 4a, the occurrence frequency of ion heating in the presence of precipitating protons is shown. The same colour scale as in Figs. 1–3 is used here. As expected, at high latitudes on the dayside (the cusp/cleft region), the conditional probability of detecting ion heating is enhanced. This can also be seen from Fig. 4b, which shows the probability of finding ion heating coexistent with suprathermal electron bursts. These electrons are generally present together with the precipitating protons in the cusp/cleft region, but also at high latitudes on the nightside. One should, moreover, note that precipitating protons can sometimes appear outside the cusp/cleft region, also in connection with ion heating (Eliasson et al., 1994a).

Accelerated auroral keV electrons are present mainly on the nightside, and they increase the probability of detecting heated ions in that region; this can be seen in Fig. 4c. In Figs. 4d and e we have plotted the probability of detecting energized ions for low ($K_p < 3-$) and high ($K_p > 4+$) magnetic activity, respectively. For high K_p indices, the probability of observing ion heating is higher for all INV and MLT,

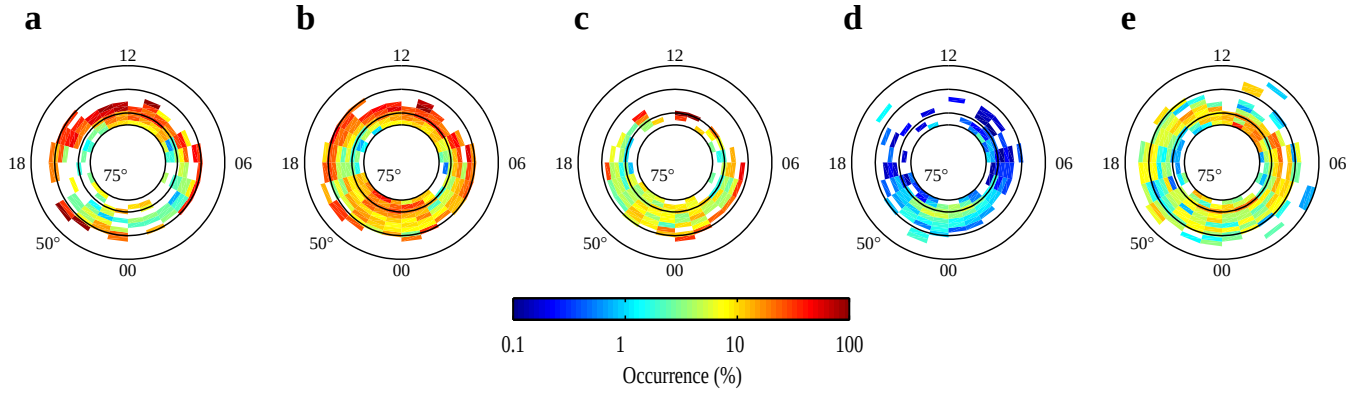

Fig. 4. Probabilities of detecting energized ions versus MLT and INV in the presence of (**a**) precipitating keV protons, (**b**) suprathermal electron bursts, (**c**) downward moving keV electrons, (**d**) low magnetic activity, $K_p < 3-$, and (**e**) high magnetic activity, $K_p > 4+$. The colour scale is the same as in Figs. 1–3.

and especially on the dayside (Yau and André, 1997). The most obvious explanation why we see an enhanced probability of finding energized ions during high magnetic activity (seen also row 11 of Table 1) is that the waves responsible for the heating are more common during high K_p indices (Yau and André, 1997).

From the above discussion we see that various wave types, particle distributions, and other characteristics seem to increase the probability of observing energized O^+ ions. However, many of these can be considered as indirect consequences of, or indirectly related to, the presence of BB-ELF waves, EMIC waves, or waves around the lower hybrid frequency, which are the main causes for the ion energization.

5.8 Ion energization by BB-ELF waves

As discussed earlier, BB-ELF waves are suitable for energizing the ions and are the main reason for the ion heating. So far, we have focused mainly on the electric wave field component of the waves. However, as we will see below, the magnetic wave field component could also be important for understanding the ion heating.

In the left column of Fig. 5 we have plotted the occurrence of BB-ELF waves versus the electric (S_E) and magnetic (S_B) field spectral densities at the oxygen gyrofrequency for all K_p (Fig. 5a), $K_p < 3-$ (Fig. 5e), and $K_p > 4+$ (Fig. 5i), respectively. The horizontal structures for low spectral densities in the left column of Fig. 5 are due to occurring artificial contributions to S_B, caused by the method of computing the spectral densities. From the original measurements, the background geomagnetic field was not properly removed, and thereafter, the Fourier spectra were computed using a rectangular window. When the magnetic wave field is low, the incomplete removal of the background field produces a spurious signal which sometimes dominates S_B. The region where some of the S_B data are contaminated with an artificial signal are indicated in Fig. 5 by shadings. Within the shaded region, some magnetic field spectral densities can be overestimated due to this artificial signal. For the data to the right of about 10^{-4} $(\mathrm{nT})^2/\mathrm{Hz}$, the effect from the artificial signal is negligible. Note also that for larger S_E, which are of importance for this study, S_B is generally higher and the contribution from the artificial signal is, therefore, insignificant.

For high magnetic activities in Fig. 5i we note a linear relation between S_E and S_B for high spectral densities. For lower K_p indices, the strong BB-ELF waves appear to have generally higher values of S_E/S_B. The dashed diagonal line indicates $S_E/S_B = c^2$, where c is the speed of light. We clearly note that there are more measurements near and to the left of this line in Fig 5e than in Fig 5i. This indicates that a larger fraction of the waves are electrostatic in nature for low magnetic activity.

In columns two and three of Fig. 5 we investigate the changes in the electron density during ion heating versus the different BB-ELF spectral densities and K_p indices presented in the first column. Figures 5b, f, and j show measurements above a sunlit ionosphere and Figs. 5c, g, and k show measurements above a dark ionosphere. The densities are averaged logarithmically in each S_E-S_B-bin and normalized to the logarithmically averaged density in the same MLT-INV-bin in the presence or absence of solar illumination. As before, the first row contains data at all K_p indices, while the middle and the last rows correspond to low and high K_p, respectively. Comparing Figs. 5b and c, we clearly see that density reductions are more common when the ionospheric foot-point of the flux tube crossed by Freja is in the shadow. Note that the density depletions in the shadow are deeper for higher S_E. This can be understood by combining Fig. 7a in André et al. (1998) and Fig. 3b in Hamrin et al. (2001): the ion energy is larger for higher electric field spectral densities, and the density reductions are deeper for larger ion energies above a dark ionosphere. One reason for the low number of observations present in Fig. 5f is that intense ion heating events during low magnetic activity on the dayside often occur on higher latitudes than 75° and, therefore, are

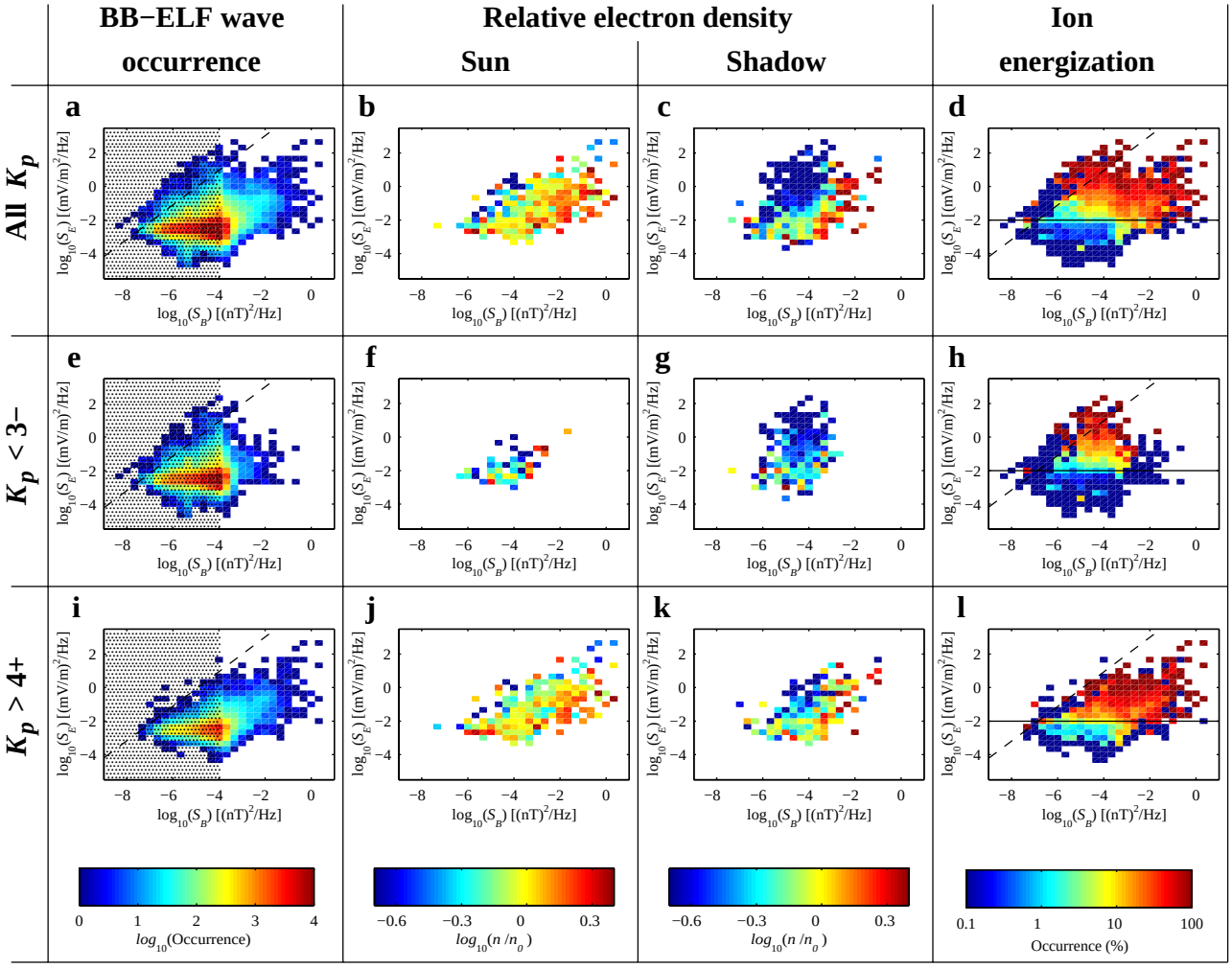

Fig. 5. The left column shows the number of measurements of BB-ELF waves versus different electric and magnetic field spectral densities (S_E and S_B) at the oxygen gyrofrequency at the Freja altitudes. The next two columns show the relative electron densities observed during ion energization events in the presence of these BB-ELF waves above a sunlit and a dark ionosphere, respectively. The probability of detecting the energized ions in the presence of the waves is shown in the last column. The top row corresponds to all K_p indices, middle row to $K_p < 3-$, and last row to $K_p > 4+$. The solid lines at $S_E = 10^{-2}$ (mV)^2/Hz in (**d**), (**h**), and (**l**) indicate the threshold used in this paper for the waves being important for the ion heating. The dashed lines in the leftmost and the rightmost columns show the location of the speed of light, $S_E/S_B = c^2$, and the shadings in (**a**), (**e**), and (**i**) indicate the regions where some of the S_B data are contaminated with an artificial signal — see the text for details.

not included in the present study (see, e.g. Plate 1, Norqvist et al., 1998).

In the absence of solar illumination and at high magnetic activity (Fig. 5k), BB-ELF waves with a high magnetic component often correspond to a density increase rather than a decrease. One explanation that we do not often observe regarding a density reduction for these waves is that the cusp/cleft region can be pushed towards the nightside during high magnetic activity. Explicit examination of some of the events included in Fig. 5k verifies this.

In the last column of Fig. 5 we have plotted the probability of detecting energized ions versus S_E and S_B for the BB-ELF waves. Assuming that the magnetic wave field component is irrelevant for the ion energization, we would expect the contours of fixed probability to be horizontal. However, by inspecting Fig. 5d we see that this is not the case. The electric field spectral density needed to cause the same amount of ion energization is lower when S_B is high than when S_B is low. Thus, the more electrostatic BB-ELF waves in Fig. 5h have a higher S_E threshold for significant ion energization than the waves in Fig. 5l. This can be seen by comparing the regions of high ion heating probability and the position of the solid line at $S_E = 10^{-2}$ (mV/m)^2/Hz.

Since the Alfvén velocity is inversely proportional to the the square root of the electron density, one would expect that data corresponding to low values of S_E/S_B originates from a sunlit ionosphere. This can be verified from Fig. 6, where we have plotted the occurrence of the BB-ELF waves and

the probability of detecting ion energization above a sunlit and a dark ionosphere, respectively. Focusing on the leftmost column in Fig. 6, we clearly note that there are more measurements near and to the left of the dashed diagonal line, (indicating the speed of light) in Fig 6c than in Fig. 6a. This cannot be explained by only changing the Alfvén velocity. Hence, this shows that a larger fraction of the waves are electrostatic in nature above an ionosphere in the shadow than one in the sunlight. Moreover, we note a resemblance between Figs. 5i and 6a and also between Figs. 5e and 6c, i.e. between high K_p indices and a sunlight ionosphere, and between low K_p indices and an ionosphere in shadow, respectively.

From Figs. 6b and d, we see that the ion energization observed above a sunlit ionosphere generally corresponds to lower values of S_E/S_B than when the ionosphere below is in the shadow. As mentioned above, intense ion heating during low magnetic activities often occurs on higher latitudes than 75° on the dayside and hence, is not included in our study. Therefore, the data presented in Fig. 6b generally correspond to a relatively high K_p (see also Fig. 5l). Also note that in Figs. 6b and d we can still see the trend previously observed in Fig. 5, that the S_E needed to cause the same amount of ion heating is lower when S_B is high than when S_B is low.

A plausible explanation for the observed importance of S_E/S_B for the ion energization is that waves can have different S_E/S_B and polarization depending on the wave vector $\boldsymbol{k}$. Furthermore, more than one wave mode can be present at the same time. Our results indicate that waves with lower S_E/S_B are more likely to fulfill the resonance conditions for ion energization.

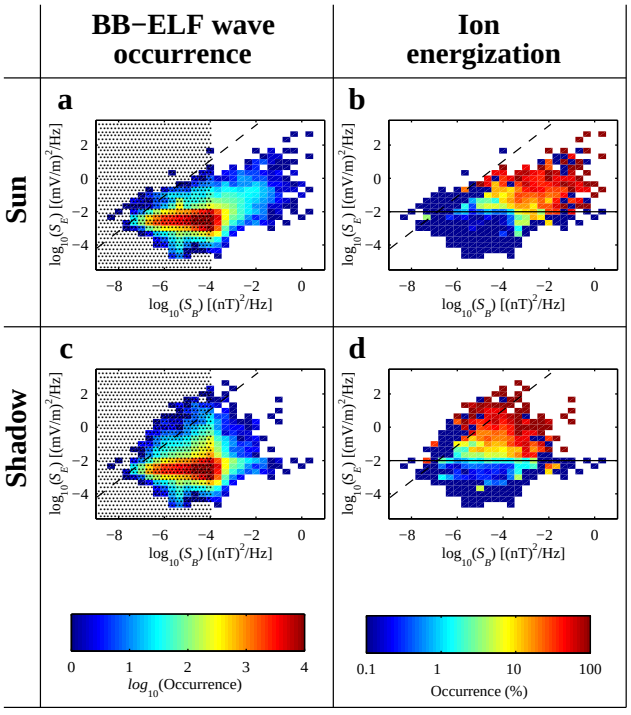

Fig. 6. The number of measurements of BB-ELF waves versus S_E and S_B at the oxygen gyrofrequency (left) and the probability of detecting energized ions in the presence of these waves (right) above a sunlit ((**a**) – (**b**)) and dark ((**c**) – (**d**)) ionosphere. The solid lines at $S_E = 10^{-2}$ (mV)^2/Hz indicate the threshold for the waves being considered important for the ion heating and the dashed lines show the location of $S_E/S_B = c^2$. The shadings indicate the regions where some of the S_B data are contaminated with an artificial signal — see the text for details.

6 Conclusions

In this paper we have presented a comprehensive statistical overview of mechanisms for the transverse energization of O^+ ions in the auroral region. We have investigated unconditionally several causes potentially relevant for the ion heating, and we have investigated conditions that are directly responsible for the heating, as well as those which are only indirectly influencing the ion energization by increasing the probability for the presence of energizing waves. The investigations in this paper help us to obtain a more exhaustive picture of the occurrence and the properties of the ion heating in the auroral region.

We have used Freja overview data of the electric and magnetic field power spectral densities, the electron number density, and the ion (O^+ and H^+) and electron count rates at, for example, various energies. The data were obtained in the Northern Hemisphere during 21 months in the declining phase of the solar cycle.

Our investigation compensates for the lack of comprehensive statistical studies in the literature. The statistical analysis simplifies the comparison between different heating mechanisms and improves the understanding of the outflow of heated ionospheric ions in the divergent geomagnetic field.

We conclude that the main cause for the energization of the oxygen ions at the Freja altitudes and latitudes is the presence of relatively strong BB-ELF waves, EMIC waves, or waves around the lower hybrid frequency. In the absence of these three wave types, ion energization is very rare.

MSC waves have also been suggested to have the ability to heat ions (Johnson et al., 1989; Le Quéau et al., 1993, 1994). However, these waves are often found to be too weak to cause intense ion heating (André et al., 1998). We find that this is consistent with our result that the MSC waves are not relevant for the ion energization.

Assuming similar spectral densities at the relevant frequencies, Chang et al. (1988) and Retterer et al. (1989) have shown that both BB-ELF waves and waves around the lower hybrid frequency are approximately equally efficient in heating ions. This is confirmed in our study. However, since BB-ELF emissions are the most frequently occurring wave type in our data, we conclude that BB-ELF waves are primarily responsible for the ion heating at Freja heights in the auroral region.

We have also identified some conditions which seem to be influencing the oxygen ion energization, but which in fact can only be considered as indirect consequences of, or in-

directly related to the presence of BB-ELF waves, EMIC waves, or waves around the lower hybrid frequency, which are primarily responsible for the ion energization. For example, the increased probability of detecting energized oxygen ions in the presence of auroral electrons can be explained by downward moving keV electrons, making the conditions favourable for the generation of the relevant waves. Likewise, precipitating protons and suprathermal electron bursts are, for example, common in the cusp/cleft region, where BB-ELF waves are also frequently occurring and ion heating is often observed.

Moreover, we have investigated the importance of the magnetic wave field component of the BB-ELF waves for the ion heating. It is found that waves with lower ratios of the spectral densities S_E/S_B are more efficient in energizing ions, possibly because they are more efficient in fulfilling the resonance condition for the heating.

Acknowledgement. We thank Liza Dackborn for developing computer codes and participating in preparing the data base used in this study. Moreover, we would like to thank Arne Moström and Olle Norberg for developing other software codes used in this study, and for helping us with computer related issues. We would also like to thank Kjell Rönnmark, Gert Brodin, and Andris Vaivads for helpful discussions and suggestions and Tanya Savitskaya for valuable help in the library. Furthermore, the PI:s of the F3H, F4, and F7 instruments, Lars Eliasson, Bengt Holback, and Manfred Boehm, are acknowledged for supplying data to this study. The Freja project is supported by the Swedish National Space Board (SNSB) and by the Deutsche Agentur für Raumfahrtangelegenheiten (DARA). The Freja satellite was managed and operated by the Swedish Space Corporation under a contract from the Swedish National Space Board.

Topical Editor M. Lester thanks R. Erlandson and another referee for their help in evaluating this paper.

References

André, M.: Dispersion surfaces, J. Plasma Phys., 33, 1–19, 1985.

André, M.: Waves and wave-particle interactions in the auroral region, J. Atmos. Sol.-Terr. Phys., 59, 1687–1712, 1997.

André, M. and Chang, T.: Ion heating perpendicular to the magnetic field, in Physics of Space Plasmas (1992), 12, pp. 35–71, Scientific Publishers Inc., Cambridge, MA, 1993.

André, M. and Yau, Y.: Theories and observations of ion energization and outflow in the high latitude magnetosphere, Space Sci. Rev., 80, 27–48, 1997.

André, M., Crew, G. B., Peterson, W. K., Persoon, A. M., Pollock, C. J., and Engebretson, M. J.: Ion heating by broad-band low-frequency waves in the cusp cleft, J. Geophys. Res., 95, 20 809–20 823, 1990.

André, M., Norqvist, P., Vaivads, A., Eliasson, L., Norberg, O., Eriksson, A. I., and Holback, B.: Transverse ion energization and wave emissions observed by the Freja satellite, Geophys. Res. Lett., 21, 1915–1918, 1994.

André, M., Norqvist, P., Andersson, L., Eliasson, L., Eriksson, A. I., Blomberg, L., Erlandson, R. E., and Waldemark, J.: Ion energization mechanisms at 1700 km in the auroral region, J. Geophys. Res., 103, 4199–4222, 1998.

Ashour-Abdalla, M., Schriver, D., and Okuda, H.: Transverse ion heating in multicomponent plasmas along auroral zone field lines, J. Geophys. Res., 93, 12 826–12 840, 1988.

Boehm, M., Paschmann, G., Clemmons, J., Höfner, H., Frenzel, R., Ertl, M., Haerendel, G., Hill, P., Lauche, H., Eliasson, L., and Lundin, R.: The TESP electron spectrometer and correlator (F7) on Freja, Space Sci. Rev., 70, 509–540, 1994.

Chang, T. and Coppi, B.: Lower hybrid acceleration and ion evolution in the suprauroral region, Geophys. Res. Lett., 8, 1253–1256, 1981.

Chang, T., Crew, G. B., Hershkowitz, N., Jasperse, J. R., Retterer, J. M., and Winningham, J. D.: Transverse acceleration of oxygen ions by electromagnetic ion cyclotron resonance with broad band left-hand polarized waves, Geophys. Res. Lett., 13, 636–639, 1986.

Chang, T., Crew, G. B., and Retterer, J. M.: Electromagnetic tornadoes in space — ion conics along auroral field lines generated by lower hybrid waves and electromagnetic turbulence in the ion-cyclotron range of frequencies, Computer Phys. Comm., 49, 61–74, 1988.

Chappell, C. R., Giles, B. L., Moore, T. E., Delcourt, D. C., Craven, P. D., and Chandler, M. O.: The adequacy of the ionospheric source in supplying magnetospheric plasma, J. Atmos. Sol.-Terr. Phys., 62, 421–436, 2000.

Desarathy, B. V.: Nearest neighbor (NN) norms: NN pattern classification techniques, IEEE Computer Society Press, 1991.

Eliasson, L., André, M., Eriksson, A., Norqvist, P., Norberg, O., Lundin, R., Holback, B., Koskinen, H., Borg, H., and Boehm, M.: Freja observations of heating and precipitation of positive ions, Geophys. Res. Lett., 21, 1911–1914, 1994a.

Eliasson, L., Norberg, O., Lundin, R., Lundin, K., Olsen, S., Borg, H., André, M., Koskinen, H., Riihelä, P., Boehm, M., and Whalen, B.: The Freja hot plasma experiment — instrument and first result, Space Sci. Rev., 70, 563–576, 1994b.

Erlandson, R. E. and Zanetti, L. J.: A statistical study of auroral electromagnetic ion cyclotron waves, J. Geophys. Res., 103, 4627–4636, 1998.

Evans, D. S.: Precipitating electron fluxes formed by a magnetic field aligned potential difference, J. Geophys. Res., 79, 2853–2858, 1974.

Gurnett, D. A. and Burns, T. B.: The low-frequency cutoff of ELF emissions, J. Geophys. Res., 73, 7437–7445, 1968.

Gurnett, D. A., Huff, R. L., Menietti, J. D., Burch, J. L., Winningham, J. D., and Shawhan, S. D.: Correlated low-frequency electric and magnetic noise along the auroral field lines, J. Geophys. Res., 89, 8971–8985, 1984.

Gustafsson, G., André, M., Matson, L., and Koskinen, H.: On waves below the local proton gyrofrequency in auroral acceleration regions, J. Geophys. Res., 95, 5889–5904, 1990.

Hamrin, M., André, M., Norqvist, P., and Rönnmark, K.: The importance of a dark ionosphere for ion heating and auroral arc formation, Geophys. Res. Lett., 27, 1635–1638, 2000.

Hamrin, M., Norqvist, P., André, M., and Eriksson, A. I.: A statistical study of wave properties and electron density at 1700 km in the auroral region, J. Geophys. Res., in press, 2001.

Holback, B., Jansson, S.-E., Åhlén, L., Lundgren, G., Lyngdal, L., Powell, S., and Meyer, A.: The Freja wave and plasma density experiment, Space Sci. Rev., 70, 577–592, 1994.

Hultqvist, B.: On the acceleration of positive ions by high-latitude, large-amplitude electric field fluctuations, J. Geophys. Res., 101, 27 111–27 121, 1996.

Johnson, J. R., Chang, T., Crew, G. B., and André, M.: Equatorially

generated ulf waves as a source for the turbulence associated with ion conics, Geophys. Res. Lett., 16, 1469–1472, 1989.

Johnstone, A. D. and Winningham, J. D.: Satellite observations of suprathermal electron bursts, J. Geophys. Res., 87, 2321–2329, 1982.

Kasahara, Y., Hosoda, T., Mukai, T., Watanabe, S., Kimura, I., Kojima, H., and Niitsu, R.: Elf/vlf waves correlated with transversely accelerated ions in the auroral region observed by akebono, J. Geophys. Res., 106, 21 123–21 136, 2001.

Kintner, P. M., Vago, J., Chesney, S., Arnoldy, R. L., Lynch, K. A., Pollock, C. J., and Moore, T. E.: Localized lower hybrid acceleration of ionospheric plasma, Phys. Rev. Lett, 68, 2448–2451, 1992.

Knudsen, D. J., Whalen, B. A., Abe, T., and Yau, A.: Temporal evolution and spatial dispersion of ion conics: evidence for a cusp heating wall, in Geophysical Monograph 84, pp. 163–169, Geophysical Monograph 84, American Geophysical Union, Washington, D. C., 1994.

Knudsen, D. J., Clemmons, J. H., and Wahlund, J.-E.: Correlation between core ion energization, suprathermal electron bursts, and broadband ELF waves, J. Geophys. Res., 103, 4171–4186, 1998.

Le Quéau, D., Roux, A., Rauch, J. L., Lefeuvre, F., and Bosqued, J. M.: Heating of protons by resonant absorption in a multicomponent plasma, 2. Theoretical model, J. Geophys. Res., 98, 13 363–13 375, 1993.

Le Quéau, D., Chust, T., and Rauch, J. L.: Ion heating by resonant absorption of electromagnetic waves in multi-ionic plasmas: A process for the formation of ion conics, J. Geomag. and Geoelec., 46, 971–985, 1994.

Lennartsson, O. W., Collin, H. L., Ghielmetti, A. G., and Peterson, W. K.: A statistical comparison of the outflow of N_2^+, NO^+ and O_2^+ molecular ions with that of atomic O^+ ions using Polar/TIMAS observations, J. Atmos. Sol.-Terr. Phys., 62, 477–483, 2000.

Lönnqvist, H., André, M., Matson, L., Bahnsen, A., Blomberg, L. G., and Erlandson, R. E.: Generation of VLF saucer emissions observed by the viking satellite, J. Geophys. Res., 98, 13 565–13 574, 1993.

Lund, E. J., Möbius, E., Carlson, C. W., Ergun, R. E., Kistler, L. M., Klecker, B., Klumpar, D. M., McFadden, J. P., Popecki, M. A., Strangeway, R. J., and Tung, Y. K.: Transverse ion acceleration mechanisms in the aurora at solar minimum: occurrence distributions, J. Atm. Sol.-Terr. Phys., 62, 467–475, 2000.

Lundin, R. and Eliasson, L.: Auroral energization processes, Ann. Geophysicae, 9, 202–223, 1991.

Lundin, R., Haerendel, G., and Grahn, S.: The Freja project, Geophys. Res. Lett., 21, 1823–1826, 1994a.

Lundin, R., Haerendel, G., and Grahn, S.: The Freja science mission, Space Sci. Rev., 70, 405–419, 1994b.

Maggs, J. E.: Coherent generation of VLF hiss, J. Geophys. Res., 81, 1707–1724, 1976.

McFadden, J. P., Carlson, C. W., Ergun, R. E., Klumpar, D. M., and Moebius, E.: Ion and electron characteristics in auroral density cavities associated with ion beams: No evidence for cold ionospheric plasma, J. Geophys. Res., 104, 14 671–14 682, 1999.

Mishin, E. and Banaszkiewicz, M.: On auroral ion conics and electron beams acceleration, Geophys. Res. Lett., 25, 4309–4312, 1998.

Newell, P. T., Meng, C., and Wing, S.: Relation to solar activity of intense aurorae in sunlight and darkness, Nature, 393, 342–344, 1998.

Norqvist, P.: Magnetospheric ion energization, Theories on observations by the Freja satellite, IRF Sci. Rep. 227, Swed. Inst. of Space Phys., Kiruna, Sweden, 1995.

Norqvist, P.: Ion energization and atmospheric outflow, Ph.D. thesis, Dep. of Space Phys., Umeå Univ., Sweden, 1998.

Norqvist, P., André, M., Eliasson, L., Eriksson, A. I., Blomberg, L., Lühr, H., and Clemmons, J. H.: Ion cyclotron heating in the dayside magnetosphere, J. Geophys. Res., 101, 13 179–13 193, 1996.

Norqvist, P., André, M., and Tyrland, M.: A statistical study of ion energization mechanisms in the auroral region, J. Geophys. Res., 103, 23 459–23 473, 1998.

Oscarsson, T., Vaivads, A., Rönnmark, K., Clemmons, J. H., de Feraudy, H., and Holback, B.: Toward a consistent picture of the generation of electromagnetic ion cyclotron ELF waves on auroral field lines, J. Geophys. Res., 102, 24 369–24 386, 1997.

Oscarsson, T., Stenberg, G., and Santolik, O.: Wave mode identification via wave distribution function analysis, Phys. Chem. Earth (C), 26, 229–235, 2001.

Rauch, J. L., Lefeuvre, F., Le Quéau, D., Roux, A., Bosqued, J. M., and Berthelier, J. J.: Heating of proton conics by resonant absorption in a multicomponent plasma, 1. Experimental evidence, J. Geophys. Res., 98, 13 347–13 361, 1993.

Retterer, J. M., Chang, T., and Jasperse, J. R.: Particle acceleration by intense auroral VLF turbulence, in: Physics of Space Plasmas, (Eds) Chang, T., Crew, G. B., and Jasperse, J. R., 9, pp. 119–160, Scientific Publishers Inc., Cambridge, MA, 1989.

Rönnmark, K.: Electron acceleration in the auroral current circuit, Geophys. Res. Lett., 26, 983–986, 1999.

Roth, I. and Hudson, M. K.: Lower hybrid heating of ionospheric ions due to ion ring distributions in the cusp, J. Geophys. Res., 90, 4191–4203, 1985.

Santolik, O. and Parrot, M.: Case studies on the wave propagation and polarization of ELF emissions observed by Freja around the local proton gyrofrequency, J. Geophys. Res., 104, 2459–2475, 1999.

Sauvaud, J.-A., Lundin, R., Rème, H., McFadden, J. P., Carlson, C., Parks, G. K., Möbius, E., Kistler, L. M., Klecker, B., Amata, E., DiLellis, A. M., Formisano, V., Bosqued, J. M., Dandouras, I., Decreau, P., Dunlop, M., Eliasson, L., Korth, A., Lavraud, B., and McCarthy, M.: Intermittent thermal plasma acceleration linked to sporadic motions of the magnetopause, first Cluster results, Ann. Geophysicae, 19, 1–11, 2001.

Sazhin, S. S. and Hayakawa, M.; Magnetospheric chorus emissions: a review, Planet. Space Sci., 40, 681–697, 1992.

Sazhin, S. S., Bullough, K., and Hayakawa, M.: Auroral hiss: a review, Planet. Space Sci., 41, 153–166, 1993.

Schunk, R. W.: Theoretical developments on the causes of ionospheric outflow, J. Atmos. Sol.-Terr. Phys., 62, 399–420, 2000.

Seki, K., Elphic, R. C., Hirahara, M., Terasawa, T., and Mukai, T.: On atmospheric loss of oxygen ions from Earth through magnetospheric processes, Science, 291, 1939–1941, 2001.

Sharp, R. D., Johnson, R. G., and Shelley, E. G.: Observation of an ionospheric acceleration mechanism producing energetic (keV) ions primarily normal to the geomagnetic field direction, J. Geophys. Res., 82, 3324–3328, 1977.

Shelley, E. G., Johnson, R. G., and Sharp, R. D.: Satellite observations of energetic heavy ions during a geomagnetic storm, J. Geophys. Res., 77, 6104–6110, 1972.

Temerin, M. and Lysak, R. L.: Electromagnetic ion cyclotron mode (ELF) waves generated by auroral electron precipitation, J. Geophys. Res., 89, 2849–2859, 1984.

Vaivads, A., André, M., Norqvist, P., Oscarsson, T., Rönnmark, K., Blomberg, L., Clemmons, J. H., and Santolik, O.: Energy transport during O+ energization by ELF waves observed by the Freja satellite, J. Geophys. Res., 104, 2563–2572, 1999.

Waldemark, J. and Norqvist, P.: In-flight calibration of satellite ion composition data using artificial intelligence methods, IRF Sci. Rep. 226, Swed. Inst. of Space Phys., Kiruna, Sweden, 1995.

Whalen, B. A., Bernstein, W., and Daly, P. W.: Low altitude acceleration of ionospheric ions, Geophys. Res. Lett., 5, 55–58, 1978.

Yau, A. W. and André, M.: Sources of ion outflow in the high latitude ionosphere, Space Sci. Rev., 80, 1–25, 1997.